An in-vivo approach to quantify in-MRI head motion tracking accuracy: comparison of markerless optical tracking versus fat-navigators

Zakaria Zariry[1,2,3], Franck Lamberton[4,5], Robert Frost[6,7], Thomas Gaass[8], Thomas Troalen[9], Holly Rayson[1,2,3], Jakob M. Slipsager[8], Nathalie Richard[1,2,3], Andre van der Kouwe[6,7], James Bonaiuto[1,2,3] and Bassem Hiba[1,2,3]

1. Institut des Sciences Cognitives Marc Jeannerod - CNRS UMR5229 - Université Lyon 1, Bron, France
2. Université Claude Bernard, Lyon 1, 69100 Villeurbanne, France
3. CNRS, Paris, France
4. Cermep, CNRS / UAR 3453, Lyon, France
5. SFR Santé Lyon-Est - CNRS UAR3453 - INSERM US7 - Université Lyon 1, Lyon, France
6. Athinoula A. Martinos Center for Biomedical Imaging, Massachusetts General Hospital, Charlestown, Massachusetts, USA
7. Department of Radiology, Harvard Medical School, Boston, Massachusetts, USA
8. TracInnovations, Ballerup, Denmark
9. Siemens Healthcare SAS, Courbevoie, France

Corresponding Author:

Dr. Bassem Hiba

Institute of Cognitive Neuroscience Marc Jeannerod,
CNRS / Université Lyon 1, UMR 5229
67 Boulevard Pinel, 69676 Bron cedex
France
E-mail : bassem.hiba@isc.cnrs.fr
Phone: +33 (0) 4 37 91 12 25

Abstract:

Purpose:

Head-motion tracking and correction remains a key area of research in MRI, but the lack of rigorous evaluation approaches hinders their optimization and comparison. This study introduces an in-vivo framework to assess head-motion tracking methods and compares a markerless optical system (MOS) to a fat-signal navigator (FatNav).

Methods:

Six participants underwent 3T brain MRI using a T1-weighted (T1w) pulse-sequence with a fat-navigator module. Participants performed head-rotations of 2° or 4°, each visually guided by MOS feedback around a single primary axis (X or Z). MOS and FatNav estimations were evaluated against T1w-images rigid-registration, as gold-standard, across seven different head positions.

Results:

The MOS outperformed FatNav in tracking primary head-rotations and unintentional translations, while FatNav showed marginally better accuracy to subtle secondary rotations. Neck-masking of fat-navigators further improved FatNav estimates of pitch^{+} rotations.

The quality of T1w-images collected motionless and with head-rotations of 2° and 4° were also investigated. The MOS outperformed FatNav in restoring image fidelity, evidenced by higher structural similarity index, peak signal-to-noise ratio and focus measure. However, image quality evaluation lacked sensitivity to subtle improvements in FatNav with neck-masking.

Conclusion:

The proposed in-vivo framework enables direct quantitative evaluation of intra-MRI head-motion tracking methods. MOS outperformed FatNav in estimating primary head rotations and unintentional translations, with a moderate FatNav advantage for small unintentional secondary rotations. Quality assessment of the motion-corrected images confirmed the superiority of MOS in practice. However, it proved less sensitive than direct comparison of movement estimates in detecting the nuanced improvements of FatNav with neck-masking.

Key words:

brain MRI, head movement tracking, markerless optical system, fat navigator, motion artifacts, motion correction.

1. Introduction

Motion artifacts represent a prevalent source of degradation in magnetic resonance imaging (MRI). When left uncorrected, they can obscure subtle pathological changes and potentially lead to the misinterpretation of clinical images[1,2]. Furthermore, these artifacts incur substantial, undesirable costs for hospitals[3]. Andre et al. estimated that repeat sequences account for 19.8% of all MRI examination performed on inpatient and/or emergency department patients[4]. This issue is particularly critical for high-resolution brain MRI, which has gained renewed interest with the advent of 7T scanners[5,6], and for imaging certain populations such as children[7].

A multitude of approaches have been proposed to mitigate head-motion artifacts during MRI acquisitions. One class of techniques relies on so-called "navigators". In brief, short acquisitions, timed before or after the echo-train at each repetition time (TR) of the imaging sequence, generate a series of low-resolution three-dimensional images of the head. These images are then registered, either prospectively or retrospectively, to estimate and compensate for head-motion at each TR. The fat navigator (FatNav) strategy employs spectrally selective RF excitation to acquire subcutaneous fat images, which serve as a head-motion navigator[8,9].

An alternative strategy involves external devices designed to monitor the head's position and orientation relative to the scanner. Such methods allow either prospective motion correction or retrospective correction of Fourier-space data using recorded motion estimations. For example, electroencephalography sensors[10], electromagnetic sensors[11] and optical tracking cameras[6,12] have been proposed to track and correct rigid head-movements during MRI. In parallel, advanced image acquisition and reconstruction techniques[13], often data-driven and increasingly powered by artificial intelligence[14,15], are also under active investigation.

Given the proliferation of head-motion correction methods in MRI, there is an urgent need for rigorous evaluation strategies that not only allow radiologists and neuroimaging researchers to appreciate the image quality benefits of each technique but also guide developers in refining their approaches. Several research groups have employed phantoms whose displacements and rotations are programmable and reproducible, with the expectation that an effective method will yield motion parameter values closely approximating the nominal values applied to the phantom[16,17]. However, the complex anatomy and composition of the human head, and its actual movements governed by complex biomechanical constraints, are not easily replicable using phantoms. Moreover, external motion sensors like optical cameras may produce different estimates for an identical movement when performed by a human head

compared to a phantom, due to inherent differences in appearance and texture. Gumus et al. found that head motion tracking errors measured in-vivo exceeded those detected in offline tests[18].

Another indirect evaluation approach involves comparing motion-corrected images with motion-free images using established image quality metrics[16,17], assessments of brain morphometric fidelity[7,16], or evaluations of how well key clinical features (e.g. lesions, anatomical boundaries) are preserved[21]. However, because this approach does not quantify the motion estimation error, it is less effective for comparing and optimizing head-motion tracking methods.

Although the development of techniques for tracking and correcting head-movements remains an essential research field in MRI, the current lack of robust in-vivo evaluation approaches impedes both their precise optimization and objective comparison. In response to this challenge, the present work introduces an in-vivo framework to evaluate head-motion tracking and correction in MRI by incorporating guided and reproducible head-movements across multiple subjects. This methodology is employed to evaluate and compare the performance of two techniques, one based on a markerless optical-system[16] (MOS) and the other on the 3D FatNav strategy[8], in six healthy subjects. By conducting this evaluation under realistic conditions, we aim to elucidate the respective strengths and limitations of each method.

2. Methods

2.1. MRI materials and participants

MRI acquisitions were conducted on a MAGNETOM Prisma 3T scanner (Siemens Healthcare, Erlangen, Germany) equipped with a 64-channel receive coil. Six healthy volunteers (31.5±6.2 years) were recruited for this study. The study protocol was in accordance with the Declaration of Helsinki, and all participants gave written informed consent which was approved by the regional ethics committee for human research (CPP Sud Mediterranee V - 2021-A00042–39). A magnetization-prepared rapid gradient echo (MP-RAGE) pulse sequence, incorporating a Fat-navigator module[9] following each TR, was employed for sagittal T1-weighted (T1w) image acquisition. Simultaneously with the MP-RAGE acquisition, head movement parameters were recorded every ~33 ms using the markerless optical device Tracoline (TCL) in combination with the TracSuite v3.3 software[22] (TracInnovations, Ballerup, Denmark). The TCL probe was positioned adjacent to the head-coil to capture part of the facial surface through the coil's aperture in front of the right eye (Figure S1-A). A cross-calibration procedure[23] to determine the transformation between optical and MRI coordinates was performed before each MRI session in accordance with the vendor's recommendations.

2.2. Motion-correction and image reconstruction

After acquisition, the Fourier-space data were transferred to a dedicated server for motion correction and image reconstruction. The RetroMocoBox toolbox[24] was then used to reconstruct the 3D fat-navigator images, before rigidly realigning them to estimate the head-movement parameters at each TR, relative to the first TR. Three sets of motion-parameters (three rotations and three translations) were computed for each MP-RAGE-image based on: 1) the original 3D fat-navigator images; 2) 3D-fat-navigator images after neck-masking[20,25]; 3) 3D fat-navigator images after masking the neck and head's occipital area. Finally, a custom pipeline inspired by the RetroMocoBox toolbox was developed in Python to apply motion-correction prior to image reconstruction. Motion transformations, estimated using either MOS or FatNav, were applied in Fourier-space after filling the missing lines via the GRAPPA algorithm[26]. The final T1w-image was obtained using a non-uniform inverse Fourier-transform.

2.3. Experimental setup and head motion control

To maintain uniform and reproducible head movements among participants, custom Python-based software was developed to provide visual instructions and feedback within the MRI environment. The 2D visual instruction animation was projected onto a screen at the back of the MRI tunnel via an external projector positioned outside the MRI room, facing a waveguide. Participants viewed the screen through a mirror mounted atop the 64-channel coil. The animation featured a white background with two main elements: 1) a red square that dynamically reflected the subject's head position, as measured in real time by the MOS system, and 2) a square with blue frame indicating the target position (Figure 1). The participant is instructed to align the red square to the blue one by adjusting their head rotations. The square's lateral displacement corresponded to rotations around the Z-axis (Rz), while its vertical movement was linked to rotations around the X-axis (Rx). Additionally, a thin black border surrounding the red square rotated according to the Y-axis rotation (Ry). A text message appeared five seconds before each movement to alert participants and prevent abrupt or forceful motions.

Additional visual instructions could be included to guide head translations along the X, Y, and Z-axes. However, to maintain participant comfort and prevent excessive instruction overload, we restricted visual guidance to head rotations only. Guided head movements are biased by the estimation errors of the MOS used in this study. Alternative real-time head tracking systems could be used to provide the required feedback on head position in the future.

Participants performed primary head rotations rightward (yaw^-), upward ($pitch^+$), and leftward (yaw^+) of 2° or 4°, each visually guided by MOS feedback around a single primary axis (X or Z). Unintentional

minor head rotations, termed secondary rotations, were observed along non-primary axes. For instance, a primary X-axis rotation also involved Y- and Z-axis secondary rotations. Similarly, head movements induce translations in all three spatial directions (Figure S2).

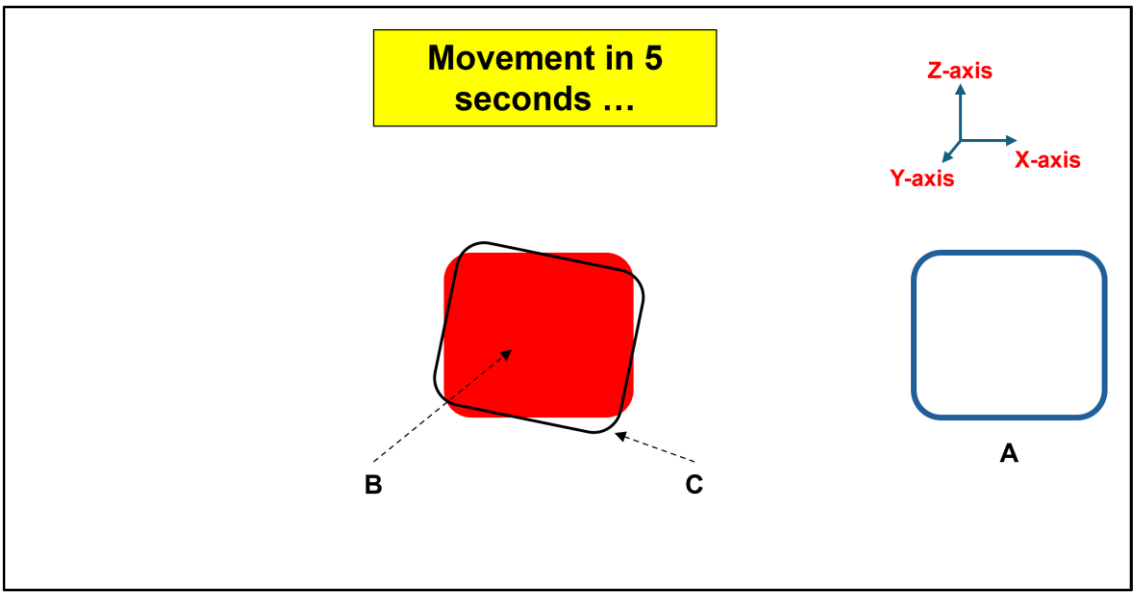

Figure 1. Visual instructions projected within the MRI to guide head rotations. The vertical and horizontal displacements of Square-A and Square-B from the isocenter correspond to the head rotations around the X- and Z-axes, respectively. Square-A indicates the target head position, whereas Square-B represents the real-time head rotation as measured by the motion tracking system (MOS). Square-C rotations, relative to Square-B, provide real-time feedback on head rotation around the Y-axis. In the present configuration, participants are instructed to perform a 4° rightward head rotation until Square-B translated horizontally to align with Square-A.

2.4. MRI experiments

2.4.1. Experiment-1: Head-motion estimation accuracy of MOS vs. FatNav

The objective of this experiment was to estimate the head position by both MOS and FatNav, in degrees and millimeters, relative to the reference position, for various stereotyped head poses. To establish a gold-standard motion estimate for a given head position, the T1w-image acquired at that position was registered to the reference image using the *mri_robust_register* FreeSurfer[27]. This procedure yields a transformation matrix describing an ideal rigid alignment between the two head positions, which is considered the gold-standard, as long as no motion occurred during acquisition of the T1w-images. Finally, the rotational and translational errors for each head-position, for both MOS and FatNav, were computed by comparing their measurements against the gold-standard estimation, as explained in Figure 2. Since the MP-RAGE pulse sequence follows a sequential phase encoding scheme, the FatNav and MOS head locations for each T1w-image were determined based on the fat-navigator location closest to the Fourier-space center sampling and the average MOS locations recorded during the five seconds nearest to this sampling.

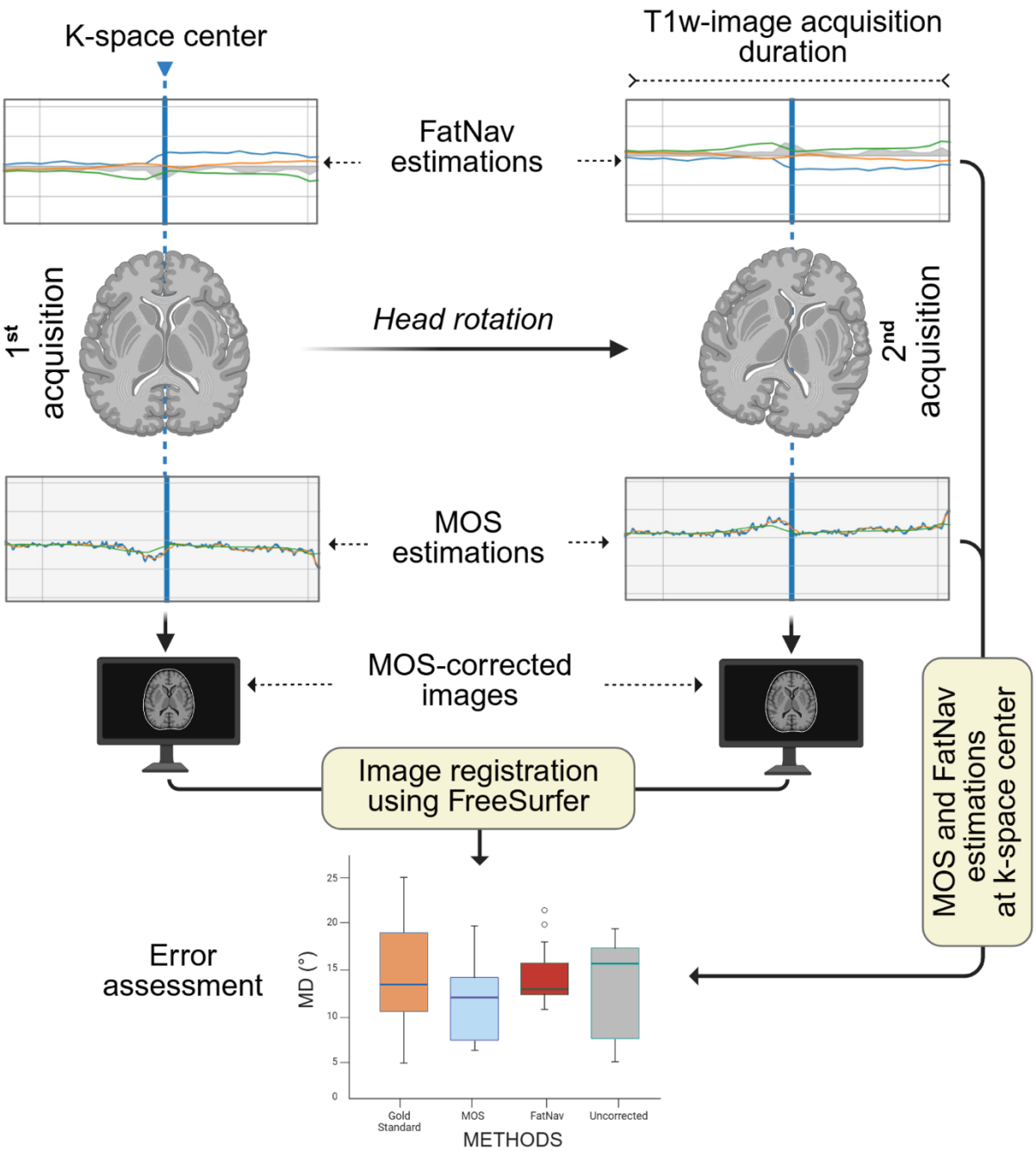

Figure 2. Procedure for assessing errors in head motion estimation by MOS and FatNav. The transformation matrices considered for MOS and FatNav are those measured during Fourier-space center sampling. FatNav and MOS head-motion estimations are compared with the gold-standard, obtained by registering each T1w-image to its reference.

Each participant underwent seven separate MP-RAGE scans with an isotropic spatial resolution of 1 mm. The imaging parameters (Table 1) were optimized to limit image-acquisition duration to 4 minutes 25 seconds, thereby reducing participant fatigue and involuntary movements. Before each T1w-scan, participants adjusted their head to a target position displayed on the screen and remained still. The first

scan, with the head straight and centered, served as a reference. Before the next three scans, participants performed specific 2° rotations relative to the reference position: rightward (yaw^-), upward ($pitch^+$), and leftward (yaw^+). These rotations were then repeated with a 4° amplitude for the final three scans.

Table 1. Parameters of sagittal T1-weighted MP-RAGE pulse sequence and its FatNav module.

Acquisition parameter	Experiment-1	Experiment-2
Isotropic resolution (mm)	1	1
Field-of-view (mm^3)	256×256×192	256×256×192
Inversion time (ms)	900	1070
Echo time (ms)	3.3	3.3
Repetition time (ms)	2180	2500
Flip angle (°)	8	8
Bandwidth (Hz/Pixel)	250	240
Parallel imaging: Acceleration factor	3×1	2×1
Parallel imaging: Nb. of ref. lines	40	32
Turbo factor	208	192
Nb. of 3D fat-navigator images	112	143
FatNav - *r*esolution (mm)	4	
FatNav - TE/TR (ms)	1.43/3.4	
FatNav - Flip angle (°)	7	
FatNav – *A*cceleration factor	4×4	
FatNav - Bandwidth (Hz/Pixel)	1950	
Total acquisition time	**4 min 9 sec**	**6 min 2 sec**

2.4.2. Experiment-2: Image quality recovery by MOS vs. FatNav

For each participant, three additional T1w-images (6 minutes each) were acquired, with settings adjusted for optimal gray to white-matter contrast (Table 1). The participant was instructed to keep their head still at the reference position for the first image. During the second acquisition, the participant was visually instructed to center their head before executing three head rotations of 2° relative to the reference position: yaw^-; $pitch^+$; and yaw^+, at 1 minute 20 seconds; 2 minute 30 seconds; and 4 minutes respectively after the scan began. The third acquisition followed the same head rotations with amplitude increased to 4°. T1w-images were each reconstructed four times using the retrospective motion-correction pipeline with motion estimates derived from MOS, FatNav, neck-masked FatNav

and FatNav with both neck- and head-occipital masking. The reference T1w-image was corrected for any unintended head-movement occurring during its acquisition using MOS estimates.

Brain extraction was then carried out using the BET[28] tool. Each T1w-image was aligned with the reference image using *mri_robust_register* to facilitate quantitative quality assessments based on three metrics: Structural Similarity Index Measure (SSIM)[29], Peak Signal-to-Noise Ratio (PSNR), and Focus Measure (Variance of Laplacian)[30]. Images were also processed with FreeSurfer 6.0[31,32] to assess the impact of the MOS and FatNav corrections on the estimation of cortical and white-matter volumes normalized by the brain volume. Finally, a visual quality evaluation of motion-corrected images was performed by three independent blinded experts who evaluated three key criteria: sharpness, noise, and ghosting artifacts, using a scoring system from 1 (poor) to 5 (excellent).

2.5. Statistical analysis

Pairwise statistical tests were performed on the estimation errors. To evaluate performance differences between MOS and FatNav, and among the three FatNav variants, a linear mixed-effects model was employed, including tracking method as a fixed effect, and subject-specific intercepts as random effects, treating different angles (2° and 4°) and directions (yaw and pitch) as repeated measures. These analyses were conducted using R (version 4.4.1)[33] and *lme4* (version 1.1.36)[34]. Fixed effects were assessed using Type II Wald F tests with Kenward-Roger estimated degrees of freedom (*car* version 3.1.3)[35]. Pairwise Tukey-corrected follow-up tests were run using estimated marginal means from the *emmeans* package (version 1.10.6)[36]. A significance threshold of $p<0.05$ was adopted. Where applicable, effect sizes (standardized mean difference, Cohen's *d*) were calculated to quantify the magnitude of the observed differences.

3. Results

3.1. Head motion reproducibility

The head-motion control strategy demonstrated high reproducibility across participants. For instructed 2° rotations, the gold-standard values were 2.09±0.39° for yaw^{-}, -1.88±0.43° for pitch^{+}, and -1.98°±0.05° for yaw^{+}. Similarly, for a 4° target head-rotation, the gold-standard values measured were 4.13±0.33°, -4.01±0.31°, and -4.08±0.22° in the respective directions. In addition to primary rotations, head translations and minor unintentional secondary head rotations were also detected (Table S1).

3.2. Head-motion estimation accuracy: MOS vs. FatNav

Figure 3 and Table 2 show results from Experiment-1 demonstrating that both MOS and FatNav with neck-masking provided head movement estimates closely approximating the gold-standard. The mean errors for primary rotations were 0.21±0.23° for MOS and 0.50±0.22° for FatNav (8.4±11.6% and 17.5±8.1% respectively). MOS showed mean errors of 0.27±0.25° for secondary rotations and 0.32±0.29 mm for translations, whereas FatNav had mean errors of 0.17±0.17° and 0.66±0.68 mm, respectively (Table S1).

Table 2. Mean ± SD values of the gold-standard and errors of MOS and FatNav (with neck-mask) for head rotations and translation estimations in Experiment-1.

Method			Yaw^+	$Pitch^+$	Yaw^-
Primary rotation	**Gold standard**	For 2° movement	**1.98±0.05°**	**1.88±0.43°**	**2.1±0.4°**
		For 4° movement	**4.08±0.22°**	**4.01±0.32°**	**4.13±0.33°**
	MOS	error (°)	0.13±0.11	0.29±0.23	0.21±0.30
	FatNav	error (°)	0.57±0.20	0.47±0.24	0.45±0.23
Secondary rotation	**Gold standard**	For 2° movement	**0.4±0.33°**	**0.33±0.36°**	**0.49±0.37°**
		For 4° movement	**0.62±0.57°**	**0.43±0.4°**	**0.66±0.51°**
	MOS	error (°)	0.2±0.1	0.24±0.25	0.36±0.33
	FatNav	error (°)	0.21±0.22	0.14±0.09	0.18±0.18
Translation	**Gold standard**	For 2° movement	**0.65±0.56 mm**	**0.59±0.37 mm**	**0.6±0.54 mm**
		For 4° movement	**1.03±1.12 mm**	**0.94±0.45 mm**	**1.04±0.91 mm**
	MOS	error (mm)	0.24±0.19	0.34±0.34	0.38±0.32
	FatNav	error (mm)	0.58±0.62	0.86±0.68	0.55±0.70

Mixed model ANOVA (α=0.05) results confirmed that MOS reduced mean primary rotation errors by 38% for $pitch^+$ (p=0.023), 77% for yaw^+ (p<0.001), and 53% for yaw^- (p=0.004) compared to FatNav, demonstrating significantly better performance. MOS also demonstrated a superior performance on translation estimation, reducing mean errors of yaw^+ by 59% (*p=0.002*) and of $pitch^+$ by 60% (*p<0.001*), compared to FatNav. In contrast, FatNav exhibited slightly better accuracy than MOS for secondary rotations during yaw^- and $pitch^+$, reducing mean errors by 50% (*p=0.014*) and 42%

($p=0.039$) respectively (Table 2 and Figure 3-A). Interestingly, MOS's ability to estimate yaw$^+$ rotation was significantly more accurate than for yaw$^-$ ($p<0.05$).

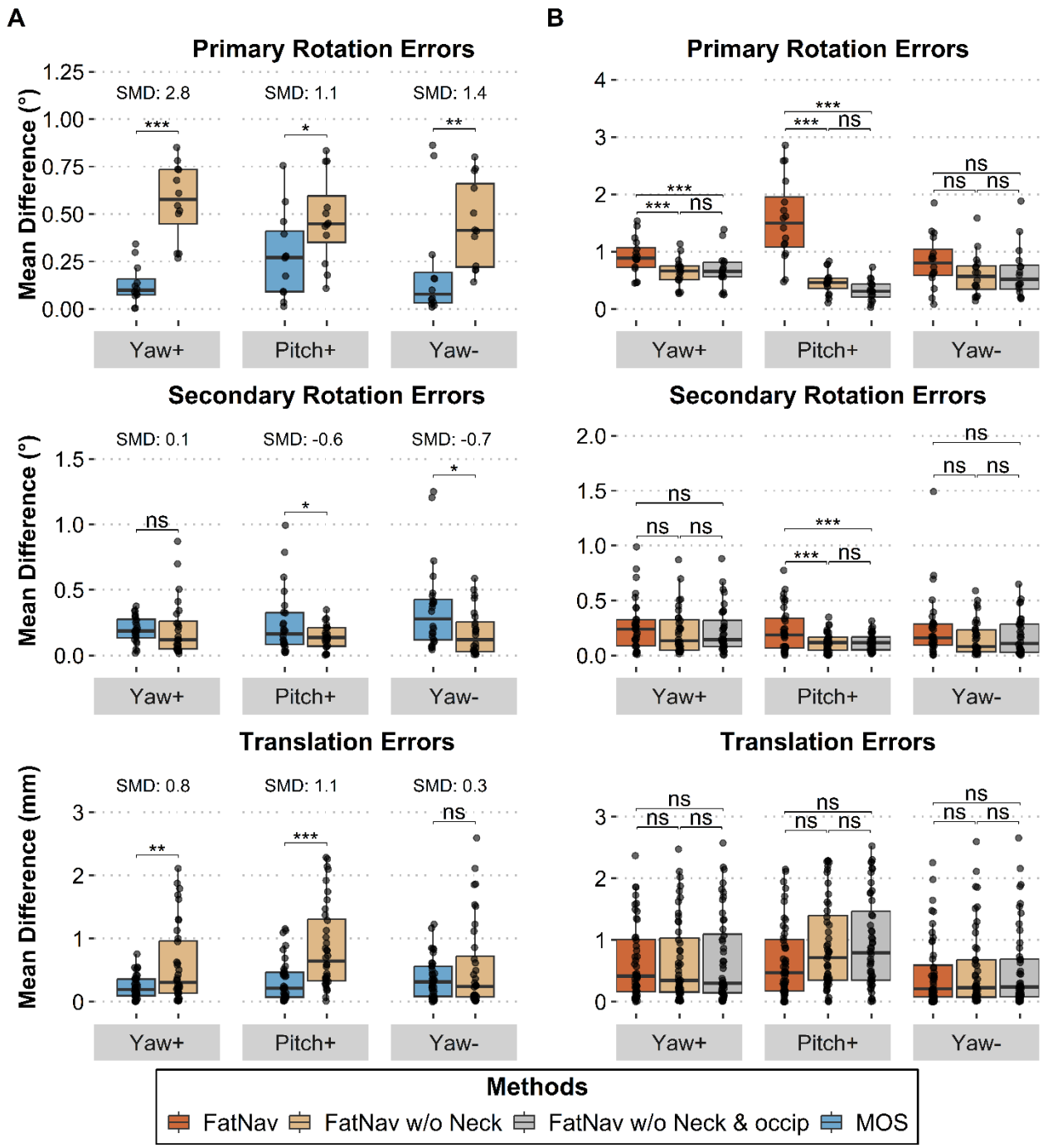

Figure 3. Accuracy of head-motion estimation: A) MOS vs. FatNav; B) FatNav with and without mask. SMD: Standardized mean difference.

Comparison of the different FatNav variants reveals that neck-masking significantly reduced the mean errors of primary and secondary pitch$^+$ rotations by respectively 48% and 32%. In contrast, masking the neck and head-occipital region did not lead to a statistically significant improvement in FatNav accuracy (Figure 3-B).

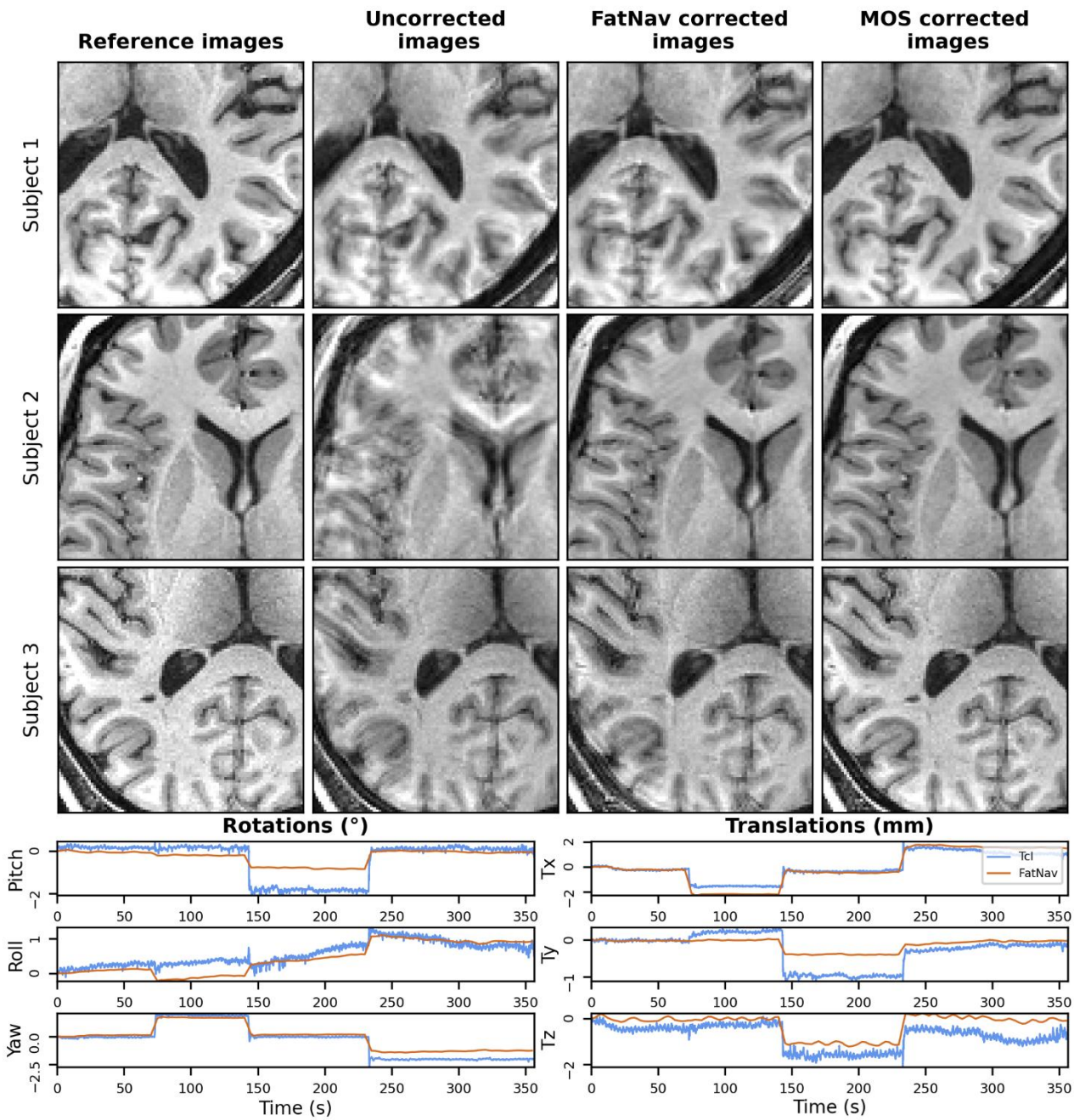

Figure 4. Visual difference between brain T1w-images of 3 volunteers without and with 2° head rotations, and the same images retrospectively corrected from motion by MOS and by FatNav with neck-mask. The curves show MOS and FatNav estimates of rotations and translations in X, Y and Z axes executed by the volunteer during one of the T1w-scans.

3.3. Image quality recovery by MOS vs. FatNav corrections

Figure 4 illustrates the impact of 2° head rotations on image quality in Experiment-2, alongside the retrospective motion correction capabilities of MOS and neck-masked FatNav. For reference, the figure also displays head rotations and translations along the X, Y, and Z axes, highlighting the

discrepancies between MOS and FatNav measurements at each time point during a 6-minute T1w-acquisition.

In blinded image quality evaluations, three evaluators assigned significantly higher scores to MOS corrected images compared to FatNav corrected images (3.58±1.13 and 2.52±0.94, respectively; *p<0.001*; Figure 5).

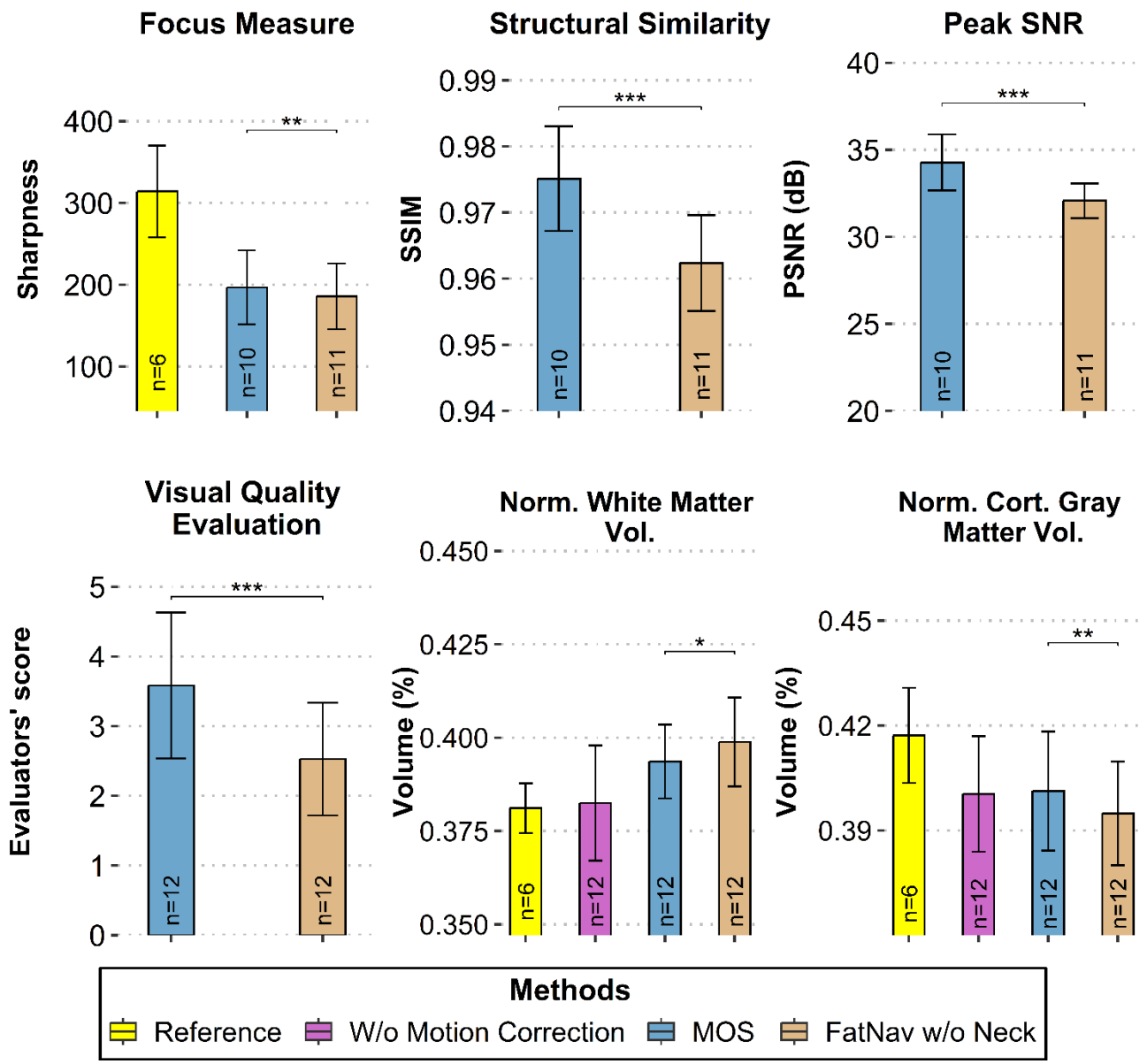

Figure 5. Visual and quantitative quality assessment of T1w-images collected in Experiment-2 and retrospectively corrected for motion effects using MOS and FatNav with neck-mask.

Quantitative analyses of image quality metrics further reinforced MOS's consistent superiority in restoring T1w-image fidelity (Figure 5). SSIM comparisons between motion-free and motion-corrected images revealed higher agreement for MOS (0.98±0.008) than for FatNav (0.96±0.007;

p<0.001). MOS also exhibited a 10.9% improvement in PSNR relative to FatNav (34.28±1.61 dB vs. 32.08±1 dB; *p*<0.001), while focus measure analyses corroborated MOS's enhancement of image sharpness (196.8±45.33 vs. 185.81±40.22; *p*=0.009; Figure 5). Notably, three T1w-images were excluded from this analysis due to anomalous SSIM values, probably due to misalignment between reference images and motion-corrected images.

Motion-artifacts systematically introduced errors in tissue volumetry (Figure 5). Relative to motion-free reference scans, uncorrected data exhibited a 4% underestimation of cortical volume and a 0.9% overestimation of white matter volume. MOS correction moderately mitigated cortical volume discrepancies (residual error: 3.8%), whereas FatNav produced less accurate cortical volumetry than uncorrected data (Figure 5). Neither correction method improved white matter quantification compared to uncorrected images.

Finally, neither visual nor quantitative evaluations of image quality revealed statistically significant performance differences between the three FatNav variants (Figure S3).

4. Discussion

This study introduces an in-vivo framework to evaluate the accuracy of intra-MRI head-motion measurements, and consequently, the effectiveness of associated correction methodologies. Custom-developed software provided real-time visual feedback via MOS to standardize head positioning, ensuring reproducible motion across participants. Moderate-to-large primary head rotations (2° and 4°) around X and Z axes were investigated. The head-movement guidance system exhibited high reproducibility and low inter-subject variability (5.6%±4.3% for 2° and 2.8%±2.1% for 4°). Head translational shifts (up to 4 mm along the X-axis during yaw rotation around Z) as well as subtle rotations around secondary non-targeted axes, consistent with natural head motion, were also observed and quantified (Table 2 and Table S1).

So far, only Gumus et al. have conducted a comparable in-vivo assessment of head motion tracking in MRI, using SPM-registration as the gold standard. However, their analysis focused solely on unguided and primary large head rotations, which exhibited high intersubject variability (37.5%, 8°±3°), and did not investigate head translations and unintentional rotations around the secondary axes[18].

In Experiment-1, motion estimates, obtained using MOS and FatNav between two head positions, were compared to the gold-standard derived from FreeSurfer's rigid registration of the corresponding image

pairs. Minor involuntary head movements during the scans could introduce differences in image quality, potentially affecting the accuracy of the rigid registration and, consequently, the gold-standard values. Even though the MOS readouts indicated only minimal involuntary movements, the Python pipeline applied the MOS estimates to reduce artifacts in the reconstructed T1w-images.

To determine whether involuntary movements affect estimation errors, we analyzed potential Spearman correlations between the mean motion-score[37] of the image pairs and the rotation and translation errors from MOS (Figure 6). The low correlation coefficients suggest that involuntary movements during the scans in Experiment-1 were unlikely to impact the accuracy of head-movement estimation extensively.

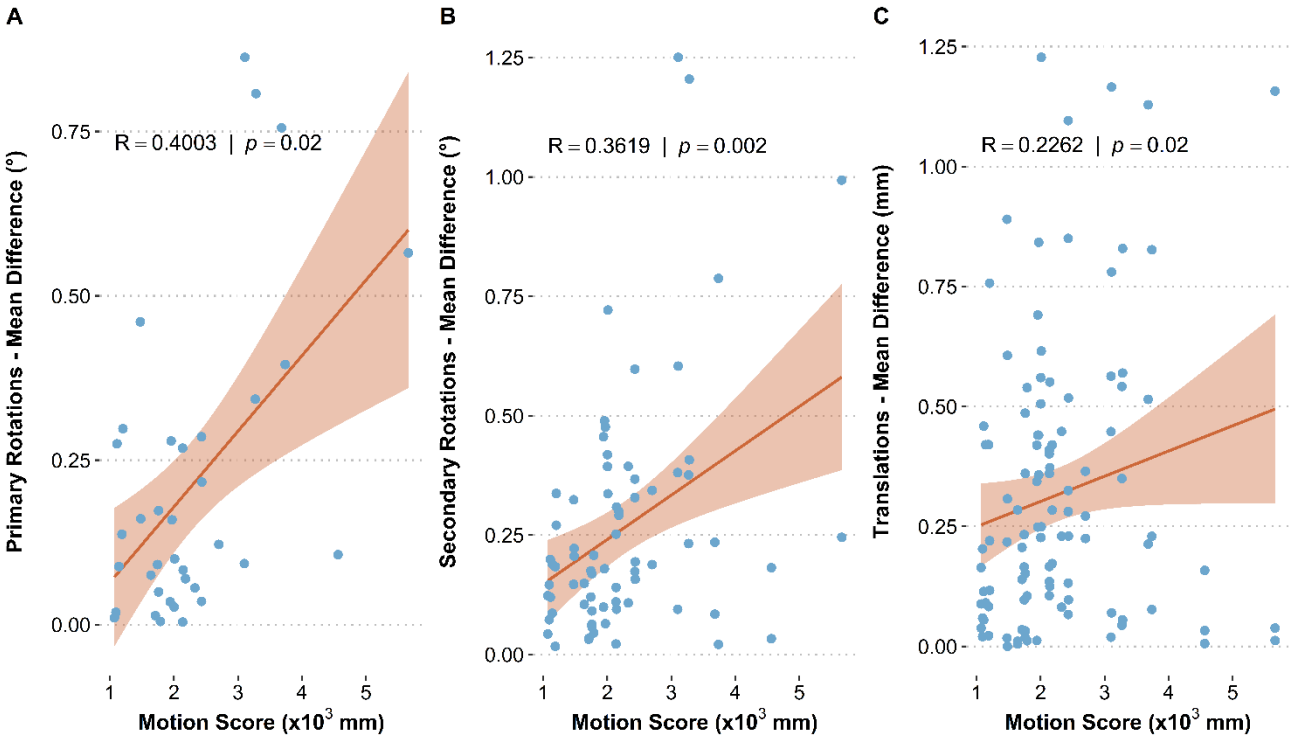

Figure 6. Spearman correlations between motion score values and the MOS errors for head motion estimation in Experiment-1.

MOS demonstrated superior accuracy than FatNav in estimating relatively large head rotations (2° and 4° amplitudes in yaw$^+$, pitch$^+$, and yaw$^-$), as well as head translational motions on two of the three movements (yaw$^+$ and pitch$^+$). Conversely, FatNav slightly outperformed MOS in the assessment of low-amplitude secondary rotations for two of the three movements (e.g., pitch$^+$ and yaw$^-$; Table 2). Further investigation is required to determine whether these MOS shortcomings are due to an intrinsic insensitivity to small-amplitude rotations or to confounding effects, where large rotations on one axis obscure the detection of smaller rotations on other axes.

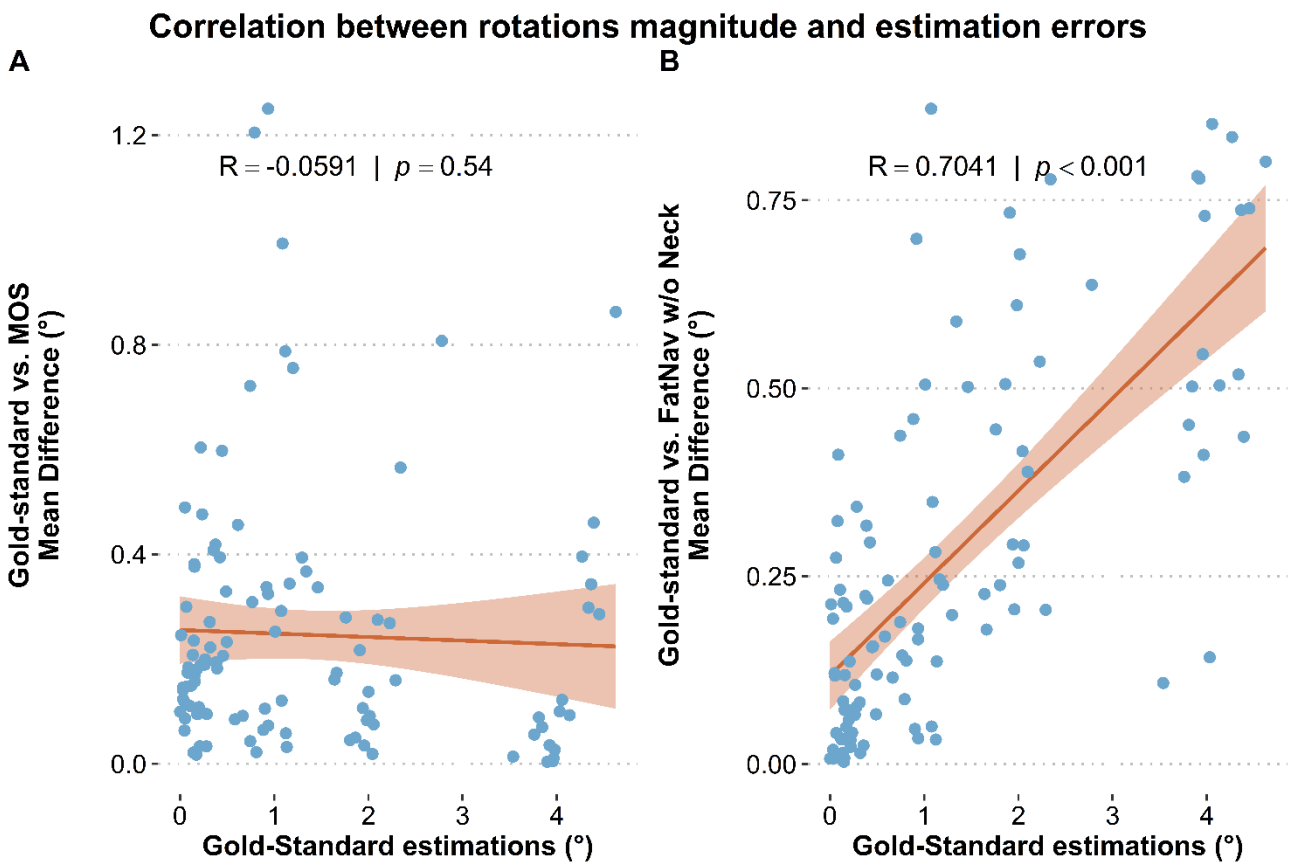

Figure 7. Spearman's rank correlation between gold-standard head rotation values and the estimation errors derived from MOS and FatNav.

Interestingly, we observe that MOS estimation errors are independent of the amplitude of head rotations (Spearman correlation R = -0.06), whereas FatNav errors increase with larger rotation amplitudes (R = 0.70; p < 0.001; see Figure 7). The reorientation of air-tissue interfaces during large head rotation relative to B0 induces substantial changes in fat-navigator image distortions. These effects, combined with elastic deformation of subcutaneous fat tissue, reduce FatNav accuracy especially in estimating X-axis rotations. This could explain the FatNav's reliable tracking of small, slow rotations but declining performance with large head-motions[18]. We emphasize that these findings are specific to our 3T FatNav implementation, different configurations may produce varying results.

The MOS appears to estimate yaw^+ better than yaw^- rotations. This could be attributable to the shifting of facial features in and out of MOS's FOV during movements. The common part of the face, useful for aligning facial surfaces over time, could therefore change according to the movement orientation and have an impact on MOS estimates.

Interestingly, the in-vivo framework presented in this study for assessing head-motion tracking was sensitive enough to detect enhancements in FatNav estimates when a neck-mask was applied to the fat-navigators. This improvement is particularly noticeable for rotations around the X axis (pitch^{+}), which causes elastic deformation at the head-neck junction (Figure 3-B). Applying head occipital masking to fat-navigator images, aimed at reducing elastic deformations of subcutaneous fat during movement, had a small, non-significant effect on FatNav performance.

In Experiment-2, participants moved their heads during each T1w-scan between four positions similar to those in Experiment-1. The head was maintained in the reference position at the start of acquisition. Yaw$^{+,}$ pitch^{+} and yaw^{-} primary rotations were performed during each T1w-scan at 1 minute 20 seconds; 2 minutes 30 seconds; and 4 minutes respectively after the start of T1w-acquisition. This choice maximizes motion-effects in the uncorrected data, while preserving the central Fourier-space sampling at pitch^{+} position. The head rotation and displacement curves, recorded during the 6-minutes T1w-acquisition (Figure 4), show discrepancies between MOS and FatNav values, consistent with the errors of both systems described in Experiment-1.

Quantitative and qualitative assessments of the quality of the T1w-images confirmed that MOS outperformed FatNav in tracking and correcting head-motion. However, this image-quality-based approach did not capture subtle performance differences between FatNav variants, making it less sensitive than the proposed in-vivo evaluation framework (Figure S3).

When compared to brain images acquired without head motion, the motion-corrected images whether using MOS or FatNav exhibited visibly lower quality (Figure 4), as corroborated by quantitative measures such as Focus Measure and the volumes of cortical and white matter (Figure 5). This degradation in image quality is attributable to the retrospective correction inherently introducing Fourier-space under-sampling/oversampling artifacts, suggesting prospective correction may yield further improvements[17].

The in vivo approach outlined here, which involves scanning immobilized heads for several minutes, does not allow for evaluating the effectiveness of MOS versus FatNav in correcting subtle, periodic head movements induced by breathing. Nevertheless, the high-frequency motion tracking provided by MOS (30 Hz vs. 1/TR=0.4 Hz for FatNav) presents an opportunity to correct for breathing motions, primarily observed as displacements along the z-axis and rotations around the x-axis[38].

We subsampled T1w-images of Experiment-1 to 2 mm isotropic resolution using trilinear interpolation, observing no significant differences in the gold-standard values of head motion estimates. This suggests that T1w-image acquisition times could be substantially shortened without

compromising the gold-standard accuracy. For instance, Gumus et al. estimated head rotation by registering anatomical images with an isotropic resolution of 2 mm, each acquired in 26 seconds[18].

Another aspect not addressed in this study is the potential for estimation errors during rapid, large-amplitude head motions, which could distort fat-navigator images and the facial surface captured by the MOS's infrared camera (Figure S1-B). This issue might be mitigated by reacquiring MRI data at the end of the T1-weighted acquisition, during motion-free intervals[37,39].

5. Conclusions

The proposed in-vivo approach using a visual feedback system for precise, reproducible motion enabled direct quantitative comparison of intra-MRI head-motion tracking and correction methods. The markerless optical system excelled in estimating head rotations and translations, while FatNav achieved only a moderate advantage in estimating unintentional small rotations around secondary axes. Although the quality assessment of motion-corrected images validated the superiority of the markerless optical system, the in-vivo approach proved more sensitive in discerning the nuanced improvements of FatNav by applying neck-masking to fat navigators. These outcomes highlight the value of in-vivo evaluation frameworks for the development and comparison of head-motion tracking and correction methods.

Acknowledgments

This work was supported by the European Research Council under the European Union's Horizon 2020 research and innovation program (ERC Consolidator Grant 864550), LABEX CORTEX funding (ANR-11-LABX-0042) from the Université de Lyon operated by the French National Research Agency (ANR), and the National Institute of Biomedical Imaging and Bioengineering (R21EB029641 and R01EB035560).

Conflict of interest statement

T.G. and J.M.S. are TracInnovations employees, and T.T. is an employee of Siemens Healthineers. All other authors declare having no competing financial and/or non-financial interests.

Data availability statement

The data and scripts that support the findings of this study are available from the corresponding author upon reasonable request.

References

1. Gedamu EL, Gedamu A. Subject movement during multislice interleaved MR acquisitions: Prevalence and potential effect on MRI-derived brain pathology measurements and multicenter clinical trials of therapeutics for multiple sclerosis. *J Magn Reson Imaging*. 2012;36(2):332-343. doi:10.1002/jmri.23666

2. Sun JP, Bu CX, Dang JH, et al. Deep learning-based reconstruction enhanced image quality and lesion detection of white matter hyperintensity through in FLAIR MRI. *Asian J Surg*. 2025;48(1):342-349. doi:10.1016/j.asjsur.2024.09.156

3. Slipsager JM, Glimberg SL, Søgaard J, et al. Quantifying the Financial Savings of Motion Correction in Brain MRI: A Model-Based Estimate of the Costs Arising From Patient Head Motion and Potential Savings From Implementation of Motion Correction. *J Magn Reson Imaging*. 2020;52(3):731-738. doi:10.1002/jmri.27112

4. Andre JB, Bresnahan BW, Mossa-Basha M, et al. Toward Quantifying the Prevalence, Severity, and Cost Associated With Patient Motion During Clinical MR Examinations. *J Am Coll Radiol*. 2015;12(7):689-695. doi:10.1016/j.jacr.2015.03.007

5. Zong X, Nanavati S, Hung S, Li T, Lin W. Effects of motion and retrospective motion correction on the visualization and quantification of perivascular spaces in ultrahigh resolution T2-weighted images at 7T. *Magn Reson Med*. 2021;86(4):1944-1955. doi:10.1002/mrm.28847

6. Gretsch F, Mattern H, Gallichan D, Speck O. Fat navigators and Moiré phase tracking comparison for motion estimation and retrospective correction. *Magn Reson Med*. 2020;83(1):83-93. doi:10.1002/mrm.27908

7. Gal-Er B, Brackenier Y, Bonthrone AF, et al. Verifying the concordance between motion corrected and conventional MPRAGE for pediatric morphometric analysis. Published online October 2, 2024. doi:10.1101/2024.10.01.616016

8. Engström M, Mårtensson M, Avventi E, Norbeck O, Skare S. Collapsed fat navigators for brain 3D rigid body motion. *Magn Reson Imaging*. 2015;33(8):984-991. doi:10.1016/j.mri.2015.06.014

9. Gallichan D, Marques JP, Gruetter R. Retrospective correction of involuntary microscopic head movement using highly accelerated fat image navigators (3D FatNavs) at 7T. *Magn Reson Med*. 2016;75(3):1030-1039. doi:10.1002/mrm.25670

10. Laustsen M, Andersen M, Xue R, Madsen KH, Hanson LG. Tracking of rigid head motion during MRI using an EEG system. *Magn Reson Med*. 2022;88(2):986-1001. doi:10.1002/mrm.29251

11. Afacan O, Wallace TE, Warfield SK. Retrospective correction of head motion using measurements from an electromagnetic tracker. *Magn Reson Med*. 2020;83(2):427-437. doi:10.1002/mrm.27934

12. Zaitsev M, Dold C, Sakas G, Hennig J, Speck O. Magnetic resonance imaging of freely moving objects: prospective real-time motion correction using an external optical motion tracking system. *NeuroImage*. 2006;31(3):1038-1050. doi:10.1016/j.neuroimage.2006.01.039

13. Cordero-Grande L, Ferrazzi G, Teixeira RPAG, O'Muircheartaigh J, Price AN, Hajnal JV. Motion-corrected MRI with DISORDER: Distributed and incoherent sample orders for reconstruction

deblurring using encoding redundancy. *Magn Reson Med*. 2020;84(2):713-726. doi:10.1002/mrm.28157

14. Yoshida N, Kageyama H, Akai H, et al. Motion correction in MR image for analysis of VSRAD using generative adversarial network. Ou Y, ed. *PLOS ONE*. 2022;17(9):e0274576. doi:10.1371/journal.pone.0274576

15. Chatterjee S, Sciarra A, Dünnwald M, Oeltze-Jafra S, Nürnberger A, Speck O. Retrospective Motion Correction of MR Images using Prior-Assisted Deep Learning. Published online November 28, 2020. doi:10.48550/arXiv.2011.14134

16. Frost R, Wighton P, Karahanoğlu FI, et al. Markerless high-frequency prospective motion correction for neuroanatomical MRI. *Magn Reson Med*. 2019;82(1):126-144. doi:10.1002/mrm.27705

17. Slipsager JM, Glimberg SL, Højgaard L, et al. Comparison of prospective and retrospective motion correction in 3D-encoded neuroanatomical MRI. *Magn Reson Med*. 2022;87(2):629-645. doi:10.1002/mrm.28991

18. Gumus K, Keating B, White N, et al. Comparison of Optical and MR-Based Tracking. *Magn Reson Med*. 2015;74(3):894-902. doi:10.1002/mrm.25472

19. Bazin PL, Nijsse HE, Van Der Zwaag W, et al. Sharpness in motion corrected quantitative imaging at 7T. *NeuroImage*. 2020;222:117227. doi:10.1016/j.neuroimage.2020.117227

20. Marchetto E, Murphy K, Glimberg SL, Gallichan D. Robust retrospective motion correction of head motion using navigator-based and markerless motion tracking techniques. *Magn Reson Med*. 2023;90(4):1297-1315. doi:10.1002/mrm.29705

21. Reuter M, Tisdall MD, Qureshi A, Buckner RL, Van Der Kouwe AJW, Fischl B. Head motion during MRI acquisition reduces gray matter volume and thickness estimates. *NeuroImage*. 2015;107:107-115. doi:10.1016/j.neuroimage.2014.12.006

22. Motion Tracking. TracInnovations. Accessed January 26, 2025. https://tracinnovations.com/motion-tracking/

23. Slipsager JM, Ellegaard AH, Glimberg SL, et al. Markerless motion tracking and correction for PET, MRI, and simultaneous PET/MRI. Zhang Q, ed. *PLOS ONE*. 2019;14(4):e0215524. doi:10.1371/journal.pone.0215524

24. retroMoCoBox/fatnavtools at master · dgallichan/retroMoCoBox. GitHub. Accessed January 26, 2025. https://github.com/dgallichan/retroMoCoBox/tree/master/fatnavtools

25. Avventi E, Ryden H, Norbeck O, Berglund J, Sprenger T, Skare S. Projection-based 3D/2D registration for prospective motion correction. *Magn Reson Med*. 2020;84(3):1534-1542. doi:10.1002/mrm.28225

26. Griswold MA, Jakob PM, Heidemann RM, et al. Generalized autocalibrating partially parallel acquisitions (GRAPPA). *Magn Reson Med*. 2002;47(6):1202-1210. doi:10.1002/mrm.10171

27. Reuter M, Rosas HD, Fischl B. Highly accurate inverse consistent registration: A robust approach. *NeuroImage*. 2010;53(4):1181-1196. doi:10.1016/j.neuroimage.2010.07.020

28. Smith SM. Fast robust automated brain extraction. *Hum Brain Mapp*. 2002;17(3):143-155. doi:10.1002/hbm.10062

29. Wang Z, Bovik AC, Sheikh HR, Simoncelli EP. Image Quality Assessment: From Error Visibility to Structural Similarity. *IEEE Trans Image Process*. 2004;13(4):600-612. doi:10.1109/TIP.2003.819861

30. Pertuz S, Puig D, Garcia MA. Analysis of focus measure operators for shape-from-focus. *Pattern Recognit*. 2013;46(5):1415-1432. doi:10.1016/j.patcog.2012.11.011

31. Fischl B, Salat DH, Busa E, et al. Whole Brain Segmentation: Automated Labeling of Neuroanatomical Structures in the Human Brain. *Neuron*. 2002;33(3):341-355. doi:10.1016/S0896-6273(02)00569-X

32. Dale AM, Fischl B, Sereno MI. Cortical Surface-Based Analysis: I. Segmentation and Surface Reconstruction. *NeuroImage*. 1999;9(2):179-194. doi:10.1006/nimg.1998.0395

33. R: A Language and Environment for Statistical Computing. Published online 2024. https://www.R-project.org/

34. Bates D, Mächler M, Bolker B, Walker S. Fitting Linear Mixed-Effects Models Using lme4. *J Stat Softw*. 2015;67:1-48. doi:10.18637/jss.v067.i01

35. Fox J, Weisberg S. *An R Companion to Applied Regression*. Third. Sage; 2019. https://www.john-fox.ca/Companion/

36. Lenth RV. emmeans: Estimated Marginal Means, aka Least-Squares Means. Published online October 20, 2017:1.10.7. doi:10.32614/CRAN.package.emmeans

37. Tisdall MD, Hess AT, Reuter M, Meintjes EM, Fischl B, Van Der Kouwe AJW. Volumetric navigators for prospective motion correction and selective reacquisition in neuroanatomical MRI. *Magn Reson Med*. 2012;68(2):389-399. doi:10.1002/mrm.23228

38. (ISMRM 2024) Hybrid Motion Correction: Latency Compensation In The Presence Of Respiratory Motion. Accessed February 12, 2025. https://archive.ismrm.org/2024/2660.html

39. Frost R, Hess AT, Okell TW, et al. Prospective motion correction and selective reacquisition using volumetric navigators for vessel-encoded arterial spin labeling dynamic angiography. *Magn Reson Med*. 2016;76(5):1420-1430. doi:10.1002/mrm.26040

Supporting materials

Figure S1. Point clouds of the facial surface captured by the markerless optical system through the coil's aperture in front of the right eye during a period of no movement (A) and during a period of significant head movement (B).

Figure S2. Primary and secondary axes of head-rotations: The primary rightward (yaw^-) and leftward (yaw^+) rotations around Z axis are associated with unintentional small secondary rotations around the Y and X axes; And the primary upward ($pitch^+$) rotation around the X axis is associated with unintentional small secondary rotations around the Y and Z axes.

Figure S3. Quality assessment of T1-weighted images acquired in Experiment-2 and retrospectively corrected for motion effects using standard FatNav, FatNav with neck-mask and FatNav with neck and head-occipital mask.

Table S1. Mean ± SD of unintentional translation and secondary rotation estimates.